Analyst

Accepted Manuscript

ROYAL SOCIETY OF CHEMISTRY

www.rsc.org/analyst

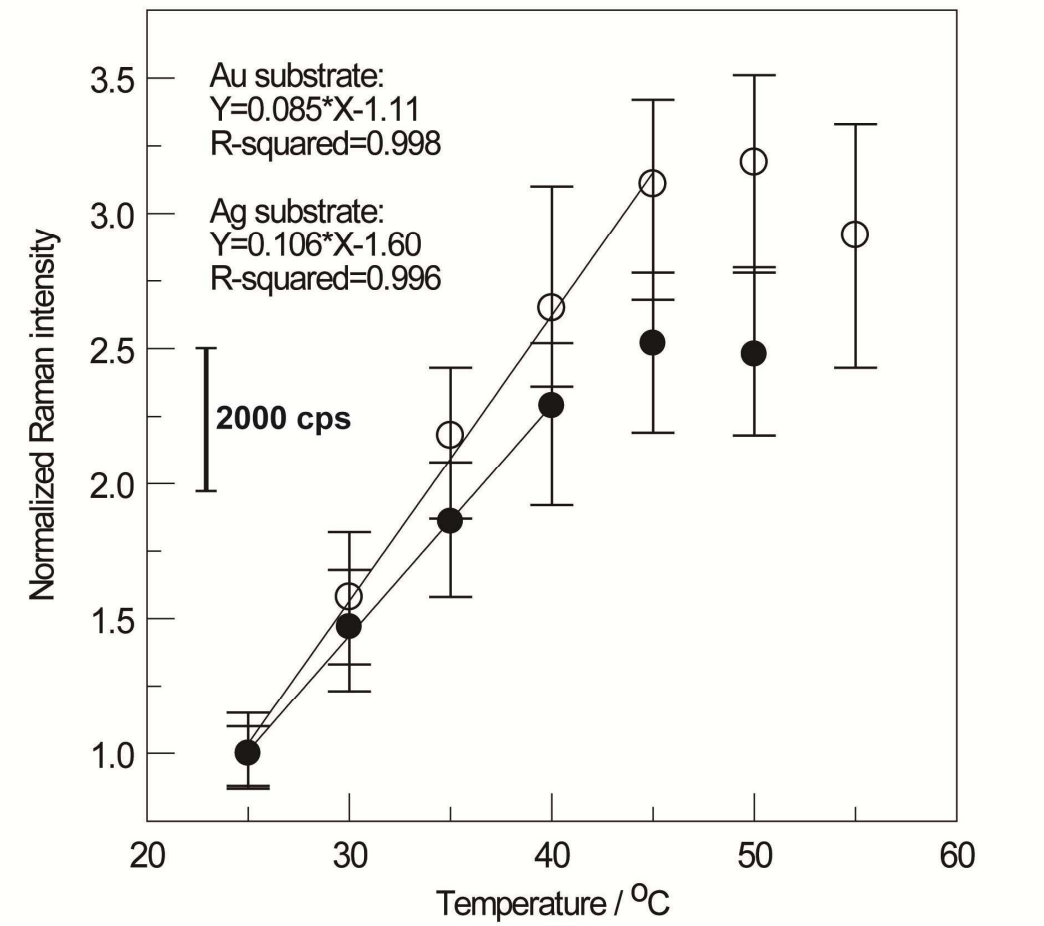

Temperature-dependent intensity is linear with a slope of ca. 430 cps / ^{o}C between 25 to 45 ^{o}C.

Room-temperature sensor based on surface-enhanced Raman spectroscopy

Kuang-Hsuan Yang,[a**] Fu-Der Mai,[b,c**] Chung-Chin Yu,[d] and Yu-Chuan Liu[b,c*]

[a]Department of Materials Science and Engineering, Vanung University, No. 1, Van Nung Road, Chung-Li City, Taiwan

[b]Department of Biochemistry, School of Medicine, College of Medicine, Taipei Medical University, No. 250, Wuxing St., Taipei 11031, Taiwan

[c]Biomedical Mass Imaging Research Center, Taipei Medical University, No. 250, Wuxing St., Taipei 11031, Taiwan

[d]Department of Environmental Engineering, Vanung University, No. 1, Van Nung Road, Chung-Li City, Taiwan

[**]These authors contributed equally to this work.

[*]Corresponding author

Tel 886-2-27361661 ext 3155; Fax 886-2-27356689; E-mail: liuyc@tmu.edu.tw

Abstract

As shown in the literature, there are many factors, including scattering cross section, polarisability and wavelength suitability, that contribute to their increased SERS

enhancement. Generally, the advantage of surface-enhanced Raman scattering (SERS)-active Ag nanoparticles (NPs) is their higher SERS enhancement over Au NPs because the molar extinction coefficient of Ag NPs is the highest one among metals. Nevertheless, the corresponding SERS-active hot spots on Au are of inherently greater stability than on Ag. In this work, innovative temperature sensors based on SERS-active Au and Ag substrates prepared by using sonoelectrochemical deposition-dissolution cycles (SEDDCs) are first reported. The SERS intensity of model probe molecules of Rhodamine 6G (R6G) adsorbed on SERS-active Ag substrate is monotonically raised from 25 to 50 ^{o}C. Moreover, this temperature-dependent intensity is linear with a slope of ca. 430 cps / ^{o}C between 25 to 45 ^{o}C. In addition, reversibility and reusability of the developed temperature sensors are evaluated after the R6G–adsorbed sensors are alternately exposed to temperatures of 25 and 45 ^{o}C in a sealed chamber. After every five cycles, SERS spectra of treated substrates were recorded and compared to those of as-prepared substrates. Experimental results indicate that the SERS enhancement capability is mostly reversible based on 90 % intensity of Raman signal being maintained for SERS-active Au substrate after 25 cycles (only 15 cycles for Ag substrate).

Introduction

Surface-enhanced Raman spectroscopy (SERS) based on well-defined localized surface plasmon resonance (LSPR) effect from Au, Ag and Cu nanoparticles (NPs) is developing as a powerful analytical tool for the extremely sensitive detection of various analytes.[1,2] The Raman effective cross sections from SERS effect are typically enhanced by 10^6~10^8 for some vibration modes of molecules in close proximity to resonant light-irradiated nano-sized metal NPs.[3,4] Thus, potential applications in various SERS-based sensors, such as glucose[5,6] and DNA[7,8] biosensors, and pH[9] and optical[10] sensors, have attracted much attentions recently. There are many factors, including scattering cross section, polarisability and wavelength suitability, that contribute to their increased SERS enhancement. As shown in the literature[11] and in our previous studies,[12,13] generally, the advantage of SERS-active Ag NPs is their higher SERS enhancement over Au NPs because the molar extinction coefficient of Ag NPs is the highest one among metals.[14] However, the disadvantage of SERS-active Ag NPs compared to Au NPs is their serious decay of SERS enhancement in ambient laboratory air.[15,16] In addition, the corresponding SERS-active hot spots on Au are of inherently greater stability than on Ag.[17,18] Therefore, we developed an electrochemical pathway to prepare SERS-active substrates with Ag underpotential deposition (UPD)-modified Au NPs to significantly enhance corresponding SERS

effects.[19] Recently, Cherukulappurath et al.[20] described a new method for rapid in situ SERS detection of ultralow subpicomolar concentration of the analyte molecules. The method is based upon a dynamic dielectrophoresis-enabled assembly of metal NPs in the form of pearl chains with nanometer-sized gaps.

On the other hand, in addition to conventional thermometer used for measuring temperature in a system, improved temperature-sensing technologies are increasingly developed in the literature.[21-23] Harada et al.[24] reported fully printed high-sensitivity multifunctional artificial electronic whiskers (e-whisker) integrated with strain and temperature sensors using printable nanocomposite inks. A supramolecular cross-linked network was fabricated and demonstrated to act as a multiple fluorescent sensor.[25] It was constructed from a fluorescent conjugated polymer and a bisammonium salt cross-linker. Thanks to the multiple stimuli-responsiveness of host–guest interactions, the fluorescence intensity of the system can be enhanced by four types of signals, including potassium cation, chloride anion, pH increase, and heating. Hence, the network can serve as a temperature sensor. Yang et al.[26] demonstrated the first application of a pyroelectric nanogenerator as a self-powered sensor (or active sensor) for detecting a change in temperature. The device consists of a single lead zirconate titanate (PZT) micro/nanowire that is placed on a thin glass

substrate and bonded at its two ends, and it is packaged by polydimethylsiloxane (PDMS).

As reported by Futamata et al.,[27] increased SERS effect at elevated temperature may result from thermal diffusion of target molecules in and out of the junctions of SERS-active metal NPs. As reported by Aggarwal et al.,[28] an increase of SERS signal upon heating was observed on a silver film over nanospheres. In our previous study,[29] the thermal degradation of polypyrrole (PPy) films was investigated by using in situ SERS. The decomposed PPy at elevated temperature reflects on its corresponding SERS spectrum. These results encourage us to innovatively develop temperature sensors based on temperature-dependent SERS signal. In our previous study,[12] we developed a simple pathway to prepare SERS-active Au substrates with excellent SERS enhancement and reproducibility by sonoelectrochemical deposition-dissolution cycles (SEDDC). In this work, we demonstrate facile room-temperature sensors based on SERS-active Au and Ag substrates prepared by SEDDC for the first time. In study, model probe molecules of Rhodamine 6G (R6G) with huge Raman cross section are employed.

Experimental Section

Chemical reagents

Electrolytes of HCl and HNO_3, and probe molecules of R6G purchased from Acros Organics were used as received without further purification. All of the solutions were prepared using deionized 18.2 MΩ cm water provided from a MilliQ system.

Preparation of SERS-active Au and Ag substrates

In electrochemical experiments, a sheet of gold (or silver) with bare surface area of 4 cm^2, a 2 ×4 cm^2 platinum sheet, and KCl-saturated silver-silver chloride (Ag/AgCl) were employed as the working, counter and reference electrodes, respectively. All the electrochemical experiments were performed in a three-compartment cell at room temperature (ca. 23^oC) and were controlled by a potentiostat (model PGSTAT30, Eco Chemie). In the oxidation-reduction cycle (ORC) treatment, the Au (or Ag) electrode was cycled in a deoxygenated 0.1 M HCl (or HNO_3 for Ag) aqueous solution from -0.28 to +1.22 (or 1.00 for Ag) V vs Ag/AgCl at a scan rate of 500 (or 50 for Ag) mV/s for 200 (or 100 for Ag) scans under slight stirring. The durations at the cathodic and anodic vertices are 10 and 5 s, respectively. After this ORC treatment, Au (or Ag)-containing complexes (precursors of metal NPs) were produced in the solution. Immediately, the treated Au (or Ag) electrode was replaced by a mechanically polished Pt substrate with a bare surface area of 0.238 cm^2 in the same solution. Then

a cathodic overpotential of 0.6 V and an anodic overpotential of 0.2 V from open circuit potential (OCP) of ca. 0.82 (or 0.95 for Ag system) V vs Ag/AgCl were applied in turn under sonication (SEDDC) to prepare SERS-active Au (or Ag) substrate. The ratio of reaction times of cathodic deposition to anodic dissolution of metal NPs is 0.2. In applying the cathodic overpotential for pulse deposition of metal NPs, the total accumulated deposition time is 2 min for every experiment. The ultrasonic treatment was performed by using an ultrasonic generator (model XL2000, Microson) and operated at 20 kHz with a barium titanate oscillator of 3.2 mm diameter to deliver a power of 80 W. The distance between the barium titanate oscillator rod and the electrode is kept at 5 mm. Finally, the prepared SERS-active substrate was took from the solution, and rinsed thoroughly with deionized water. Then it was dried in a vacuum-dryer with dark atmosphere for 1 h at room temperature for subsequent use.

SERS measurements on SERS-active substrates

In SERS measurements, 20 μL R6G with concentration of 2×10^{-6} M was directly dropped on the as-prepared SERS-active substrates by using a pipette from a working solution of 100 mL. After 30 min for equilibrium the R6G-adsorbed substrates were rinsed thoroughly with deionized water to remove any unbound R6G. Finally they were dried in a dark vacuum-dryer for 1 h at room temperature for subsequent tests.

SERS-active substrates at different temperatures were prepared by mounting the samples on a thermal heater (THMS 600, Linkam Scientific Instruments, UK) at a heating rate of 1 ^{o}C/min in air. Before heating, the chamber of the sealed thermal heater was deoxygenated with highly pure nitrogen.

Characterization of SERS-active substrates

The surface morphologies of metal substrates were examined by using scanning electron microscopy (SEM, model S-4700, Hitachi, Japan). In situ Raman spectrum was obtained (Renishaw InVia Raman spectrometer) by using a confocal microscope employing a diode laser operating at 785 nm with an output power of 1 mW on the heated sample. The excitation wavelength of 785 nm is a particular choice for avoiding interference from the electronic transition of model probe molecule of R6G. A 50x, 0.50 NA Leica objective with long working-distance was used to focus the laser light on the samples. The laser spot size is ca. 1~2 μm. A thermoelectrically cooled charge-coupled device (CCD) 1024 x 256 pixels operating at -60 ^{o}C was used as the detector with 1 cm^{-1} resolution. All spectra were calibrated with respect to silicon wafer at 520 cm^{-1}. In measurements, the laser beam was focused down to the objective lens. The backscattered Raman signal was collected by the same objective lens and passed through an adjustable confocal hole to filter the unexpected stray-light

noise. A holographic notch filter was used to filter the excitation line from the collected light. The acquisition time for each measurement was 10 s. Replicate measurements of five times on different areas were made to verify the spectra were a true representation of each sample. The SERS effect was evaluated on the strongest band intensity of R6G at ca. 1510 cm^{-1} on the Raman spectrum. The normalized band intensity of R6G at ca. 1510 cm^{-1} was obtained by subtracting this band from the nearby background at ca. 1407 cm^{-1}. An average band intensity was determined from five measurements on each sample.

Results and discussion

Surface morphologies of SERS-active substrates at different temperatures

The recognized mechanisms on SERS consist of two major components, electromagnetic (EM) enhancement[30,31] and chemical (CHEM) enhancement.[32,33] EM enhancement results from the enhancement of local electromagnetic fields at the surface of a metal which can support surface plasma/optical conduction resonances. CHEM enhancement is associated with the charge transfer between the metal and adsorbate at atomic-scale roughness features. In contrast to the well known EM, the CHEM remains much more enigmatic and hard to ascertain. Fig. 1a shows the

microstructure of the Au NPs-deposited substrate at 25 °C without treatment by heating. Clearly, the surface morphology demonstrates a typical aspect of rough surface with microstructure smaller than 100 nm, which is suitable for Raman spectrum-related study.[34,35] Meanwhile, densely packed sphere Au NPs were observed on the Au substrate, which was consistent with the surface morphology shown in our previous study.[12] With the further heating treatment to Au NPs on the substrate from 25 to 45 °C, the surface morphology was not significantly changed, as shown in Fig. 1b. It suggests that this heating treatment to SERS-active substrate doesn't demonstrate significant influence on the corresponding SERS effect from the viewpoint of EM enhancement. Because molecules located between two metallic NPs display the greatest SERS enhancement[36,37] this conclusion is based on the shapes and densities of metal NPs deposited on substrates are slightly different at different temperatures. Similarly, this heating treatment to Ag NPs-deposited substrate from 25 to 50 °C doesn't demonstrate significant influence on the corresponding SERS effect, as revealed from the less change in surface morphologies at different temperatures (Figs. 2a and 2b). Therefore, the explanation of the improved SERS effect observed on metal substrates at elevated temperatures is further considered from the viewpoint of CHEM enhancement, as discussed later.

Temperature-dependent SERS intensities on metal NPs-deposited substrates

To examine the temperature-dependent SERS intensities on metal NPs-deposited substrates model probe molecules of R6G with huge Raman cross section were used. In addition, to isolate this temperature effect on SERS effect form resonance-enhanced Raman scattering (RRS)[38] effect diode laser light of 785 nm was used in this work. Fig. 3 shows the temperature effect of Au NPs-deposited substrate on the corresponding SERS effects (spectrum a for a reference temperature of 25 ^{o}C; while spectrum b for an elevated temperature of 45 ^{o}C). As shown in spectrum b of Fig. 3, it is characteristic of Raman spectrum of R6G.[39-41] The band at ca. 611 cm^{-1} is assigned to the C-C-C ring in-plane vibration mode. The band at ca. 768 cm^{-1} is assigned to the C-H out-of-plane bend mode. The bands at ca. 1127 and 1182 cm^{-1} are assigned to the C-H in-plane bend modes. The bands at ca. 1311 and 1574 cm^{-1} are assigned to the N-H in-plane bend modes. The bands at ca. 1363, 1511 and 1650 cm^{-1} are assigned to the C-C stretching modes. Interestingly, when spectrum b of Fig. 3 (at 45 ^{o}C) was compared with spectrum a of Fig. 3 (at 25 ^{o}C), it was clearly found that the spectral relative intensity can be enhanced by ca. 1.5-fold of magnitude due to the contribution from heating effect. Further thermal gravity analysis experiment indicated that decomposition of R6G below 100 °C is negligible. In calculating the relative intensity, we employ the normalized Raman intensity, which is calculated

from the ratio of the strongest intensity of R6G adsorbed on SERS-active Au substrate at elevated temperature to that of R6G adsorbed on the same SERS-active Au substrate at 25 ^{o}C. Thus, no correction to the normal Raman scattering intensity is necessary to account for differences in sampling geometry and scattering phenomena.[42] This similar temperature effect on the correspondingly improved SERS effect is more significantly observed on the SERS-active Ag substrate, as shown in Fig. 4. When spectrum b of Fig. 4 (at 50 ^{o}C) was compared with spectrum a of Fig. 4 (at 25 ^{o}C), it was clearly found that the spectral relative intensity can be enhanced by ca. 2.2-fold of magnitude due to the contribution from heating effect. In this system, increasing the temperature of substrates, the increased SERS enhancement capability may be ascribed to the charge transfer between probe molecules of R6G and SERS-active metal substrate, which is responsible for the chemical effect of SERS mechanisms, because the contribution from EM enhancement is hard to be evaluated for this improved SERS effect, as indicated before in Figs. 1 and 2. This increased SERS effect at elevated temperature may result from thermal diffusion of individual R6G molecules in and out of the junctions of SERS-active metal NPs with effective enhancement in SERS.[27] Since the EM enhancement is far greater than the CHEM enhancement the improved SERS effects at elevated temperatures observed on SERS-active Au and Ag substrates are not significant. However, this

substrate-temperature dependence of SERS above room temperature can be applicable in temperature sensor, as discussed later.

SERS temperature sensors on metal NPs-deposited substrates

To examine the observed substrate-temperature dependence of SERS above room temperature as a promising temperature sensor, the R6G-adsorbed SERS-active substrate was stepwise heated from 25 to 50 °C (for Au substrate) and to 55 °C (for Ag substrate). Fig. 5 exhibits the corresponding substrate-temperature dependences of SERS intensities of R6G adsorbed on Au and Ag substrates. As seen in Fig. 5 for Au substrate (solid circle), the normalized Raman intensity of R6G increases with the increasing temperature of the heated substrate. This increased normalized intensity reaches to a maximum value of 2.5 times at 45 °C. Then the normalized intensity slightly decreases at a higher temperature of 50 °C. Similar phenomenon was also observed on the SERS-active Ag substrate (hollow circle). This increased normalized intensity reaches to a maximum value of 3.2 times at 50 °C. Then the normalized intensity decreases at a higher temperature of 55 °C. Be a SERS temperature sensor this substrate-temperature dependence of SERS should be linear. Thus, the linear regression equation was made between 25 and 40 °C for SERS-active Au substrate (between 25 and 45 °C for SERS-active Ag substrate). The obtained equation is y =

0.085x−1.11 for Au substrate (y = 0.1.06x−1.60 for Ag substrate), where y and x represent normalized Raman intensity and temperature (^{o}C), respectively. The correlation coefficient is 0.998 for Au substrate (0.996 for Ag substrate), which suggests a good linear relationship between normalized Raman intensity of probe molecule and substrate temperature. The slope in this linear equation represents the sensitivity of a temperature sensor. Obviously, the SERS temperature sensor based on Ag substrate (ca. 430 cps / ^{o}C) performances more sensitively than that based on Au substrate (ca. 340 cps / ^{o}C) does.

Besides the sensitivity, the stability is also an important factor that should be carefully considered in development of sensors. In this work, the reusability is evaluated after the R6G–adsorbed sensors are alternately exposed to temperatures of 25 and 45 ^{o}C in a sealed chamber. After every 5 cycles, the corresponding SERS intensities were measured at 25 ^{o}C and compared with the SERS intensity measured on as-prepared SERS-active substrate. As shown in Fig. 6 for Au substrate (solid circle), the SERS enhancement capability is mostly reversible based on 90 % intensity of Raman signal being maintained after 25 cycles. However, the SERS enhancement capability is mostly reversible based on 90 % intensity of Raman signal being maintained after only 15 cycles for Ag substrate (hollow circle). The slight increase in the SERS enhancement capability before 10 cycles observed on both Au and Ag

substrates is interesting and was also similarly reported in glucose biosensor based on SERS.[43] Accordingly, the advantage of this developed temperature sensor based on SERS-active Ag substrate is its good sensitivity. On the other hand, the advantage of this developed temperature sensor based on SERS-active Au substrate is its good stability.

Conclusions

In this work, temperature sensors between 25 and 45 ^{o}C based on SERS-active Au and Ag substrates were prepared by using electrochemical technique of SEDDCs. The advantage of this developed temperature sensor based on SERS-active Ag substrate is its good sensitivity with 430 cps / ^{o}C. The advantage of this developed temperature sensor based on SERS-active Au substrate is its good stability with reusability after testing for 25 cycles. Utilizing the advantages of higher SERS enhancement from Ag NPs and higher SERS stability from Au NPs in developing SERS temperature sensor with both high sensitivity and excellent stability are underway.

Acknowledgments

The authors thank the National Science Council of the Republic of China and Taipei Medical University for their financial support.

References

1 Y. Wang, X. Zhang, P. Gao, Z. Shao, X. Zhang, Y. Han and J. Jie, *ACS Appl. Mater. Interfaces*, 2014, **6**, 977.

2 S. R. Panikkanvalappil, M. A. Mahmoud, M. A. Mackey and M. A. El-Sayed, *ACS Nano*, 2013, **7**, 7524.

3 J. A. Dieringer, A. D. McFarland, N. C. Shah, D. A. Stuart, A. V. Whitney, C. R. Yonzon, M. A. Young, Zhang and R. P. Van Duyne, *Faraday Discuss.*, 2006, **132**, 9.

4 K. L. Ou, T. C. Hsu, Y. C. Liu, K. H. Yang and H. Y. Tsai, *Anal. Chim. Acta*, 2014, **806**, 188.

5 K. Ma, J. M. Yuen, N. C. Shah, J. T. Walsh, Jr. M. R. Glucksberg and R. P. Van Duyn, *Anal. Chem.*, 2011, **83**, 9146.

6 C. R. Yonzon, D. A. Stuart, X. Zhang, A. D. McFarland, C. L. Haynes and R. P. Van Duyne, *Talanta*, 2005, **67**, 438.

7 M. Li, J. Zhang, S. Suri, L. J. Sooter, D. Ma and N. Wu, *Anal. Chem.*, 2012, **84**, 2837.

8 K. Chen, H. Han, Z. Luo, Y. Wang and X. Wang, *Biosen. Bioelectron.*, 2012, **34**, 118.

9 V. T. Cong, E. O. Ganbold, J. K. Saha, J. Jang, J. Min, J. Choo, S. Kim, N. W. Song, S. J. Son, S. B. Lee and S. W. Joo, *J. Am. Chem. Soc.*, 2014, **136**, 3833.

10 V. López-Puente, S. Abalde-Cela, P. C. Angelomé, R. A. Alvarez-Puebla, L. M. Liz-Marzán, *J. Phys. Chem. Lett.*, 2013, **4**, 2715.

11 W. Hsiao, H. Chen, Y. Yang, Y. Chen, C. Lee and H. Chiu, *ACS Appl. Mater. Interface*, 2011, **3**, 3284.

12 F. D. Mai, T. C. Hsu, Y. C. Liu, K. H. Yang and B. C. Chen, *Chem. Commun.*, 2011, **47**, 2958.

13 C. C. Chang, K. H. Yang, Y. C. Liu and C. C. Yu, *Anal. Chim. Acta*, 2012, **709**, 97.

14 T. A. Taton, C. A. Mirkin and R. L. Letsinger, *Science*, 2000, **289**, 1760.

15 N. L. Rosi and C. A. Mirkin, *Chem. Rev.*, 2005, **105**, 1562.

16 M. D. Mcmahon, R. Lopez, H. M. Meyer III, L. C. Feldman and R. F. Haglund JR, *Appl. Phys. B*, 2005, **80**, 921.

17 P. Gao and M. J. Weaver, *J. Phys Chem.*, 1985, **89**, 5046.

18 P. Gao, D. Gosztola, L. W. H. Leung and M. J. Weaver, *J. Electroanal. Chem.*, 1987, **23**, 222.

19 C. C. Chang, K. H. Yang, Y. C. Liu, C. C. Yu and Y. H. Wu, *Analyst*, 2012, **137**, 4943.

20 S. Cherukulappurath, S. H. Lee, A. Campos, C. L. Haynes and S. H. Oh, *Chem. Mater.*, 2014, **26**, 2445.

21 C. Gómez-Polo, J. Soto-Armañanzas, J. Olivera, J. I. Pérez-Landazábal, S. Larumbe, M. A. Miranda, C. A. de la Cruz, I. Mendizábal, S. A. Korili and A. Gil, *Ind. Eng. Chem. Res*., 2013, **52**, 3787.

22 P. Neumann, I. Jakobi, F. Dolde, C. Burk, R. Reuter, G. Waldherr, J. Honert, T. Wolf, A. Brunner, J. H. Shim, D. Suter, H. Sumiya, J. Isoya, J. Wrachtrup, *Nano Lett.*, 2013, **13**, 2738.

23 Y. Nakasone, T. Ono, A. Ishii, S. Masuda, M. Terazima, *Biochemistry*, 2010, **49**, 2288.

24 S. Harada, W. Honda, T. Arie, S. Akita, K. Takei, *ACS Nano*, DOI: 10.1021/nn500845a.

25 X. Ji, Y. Yao, J. Li, X. Yan and F. Huang, *J. Am. Chem. Soc.*, 2013, **135**, 74.

26 Y. Yang, Y. Zhou, J. M. Wu and Z. L. Wang, *ACS Nano*, 2012, **6**, 8456.

27 M. Futamata, Y. Maruyama and M. Ishikawa, *J. Phys. Chem. B*, 2004,**108**, 13119

28 R. L. Aggarwal, L. W. Farrar and S. K. Saikin, *J. Phys. Chem. C*, 2012, **116**, 16656.

29 Y. C. Liu, K. H. Yang, L. H. Lin and J. F. Tsai, *Electrochem. Commun.*, 2008, **10**, 161.

30 D. H. Jeong, Y. X. Zhang and M. Moskovits, *J. Phys. Chem. B*, 2004, **108**, 12724.

31 M. Li, S. K. Cushing, H. Liang, S. Suri, D. Ma and N. Wu, *Anal. Chem.*, 2013, **85**, 2072.

32 M. Baibarac, I. Baltog, S. Lefrant, J. Y. Mevellec and O. Chauvet, *Chem. Mater.*, 2003, **15**, 4149.

33 Y. C. Liu, K. H. Yang and T. C. Hsu, *Anal. Chim. Acta*, 2009, **636**, 13.

34 G. Cardini, M. Maurizio-Miranda and V. J. Schettino, *J. Phys. Chem. B*, 2004, **108**, 17011.

35 E. Hesse and J. A. Creighton, Langmuir, 1999, **15**, 3550.

36 Y. H. Kim, D. K. Lee, H. G. Cha, C. W. Kim and Y. S. Kang, *J. Phys. Chem. C*, 2007, **111**, 3629.

37 I. Pockrand,*Chem. Phys. Lett*., 1982, **85**, 37.

38 N. Stürzl, S. Lebedkin, S. Klumpp, F. Hennrich and M. M. Kappes, *Anal. Chem.*, 2013, **85**, 4554.

39 Y. Lu, G. L. Liu and L. P. Lee, *Nano Lett.*, 2005, **5**, 9.

40 Z. Sun, Y. Li, Y. Wang, X. Chen, J. Zhang, K. Zhang, Z. Wang, C. Bao, J. Zeng, B. Zhao and B. Yang, *Langmuir*, 2007, **23**, 10731.

41 L. Jensen and G. C. Schatz, *J. Phys. Chem. A*, 2006, **110**, 5977.

42 C. E. Taylor, J. E. Pemberton, G. G. Goodman and M. H. Schoenfisch, *Appl. Spectrosc.*, 1999, **53**, 1221.

43 C. R. Yonzon, C. L. Haynes, X. Zhang, J. T. Walsh and R.P. Van Duyne, *Anal. Chem.*, 2004, **76**, 78.

Figure Captions

Fig. 1. SEM images of SERS-active Au substrates treated at different temperatures: (a) 25 ^{o}C; (b) 45 ^{o}C.

Fig. 2. SEM images of SERS-active Ag substrates treated at different temperatures: (a) 25 ^{o}C; (b) 50 ^{o}C.

Fig. 3. SERS spectra of 2 × 10^{-6} M R6G adsorbed on SERS-active Au substrate treated at different temperatures: (a) 25 ^{o}C; (b) 45 ^{o}C.

Fig. 4. SERS spectra of 2 × 10^{-6} M R6G adsorbed on SERS-active Ag substrate treated at different temperatures: (a) 25 ^{o}C; (b) 50 ^{o}C.

Fig. 5 Normalized Raman intensities of 2 × 10^{-6} M R6G adsorbed on SERS-active Au (solid circle) and Ag (hollow circle) substrates treated at different temperatures. The average band intensity was determined from five measurements on each sample. The error bars were decided by using the maximum and minimum values in the five measurements.

Fig. 6. Normalized Raman intensities of 2 × 10^{-6} M R6G adsorbed on SERS-active Au (solid circle) and Ag (hollow circle) substrates treated between 25 and 45 ^{o}C for different cycles. The average band intensity was determined from five measurements on each sample. The error bars were decided by using the maximum and minimum values in the five measurements.

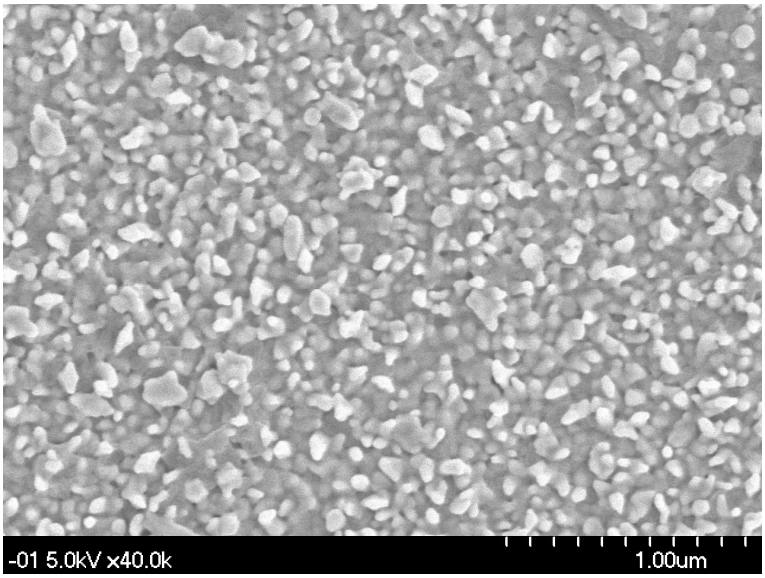

(a)

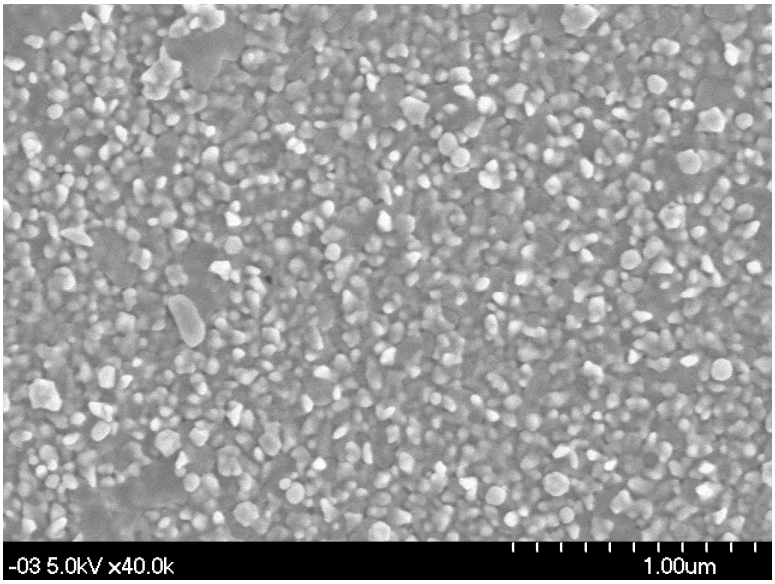

(b)

Fig. 1.

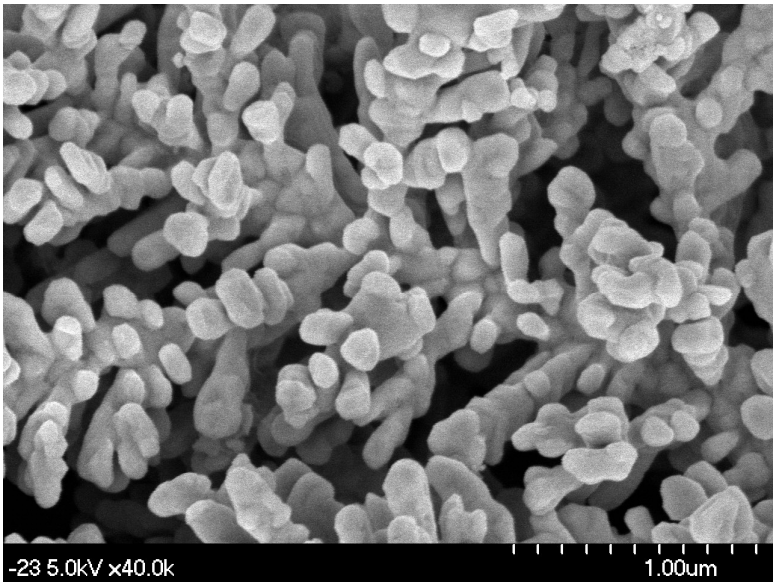

(a)

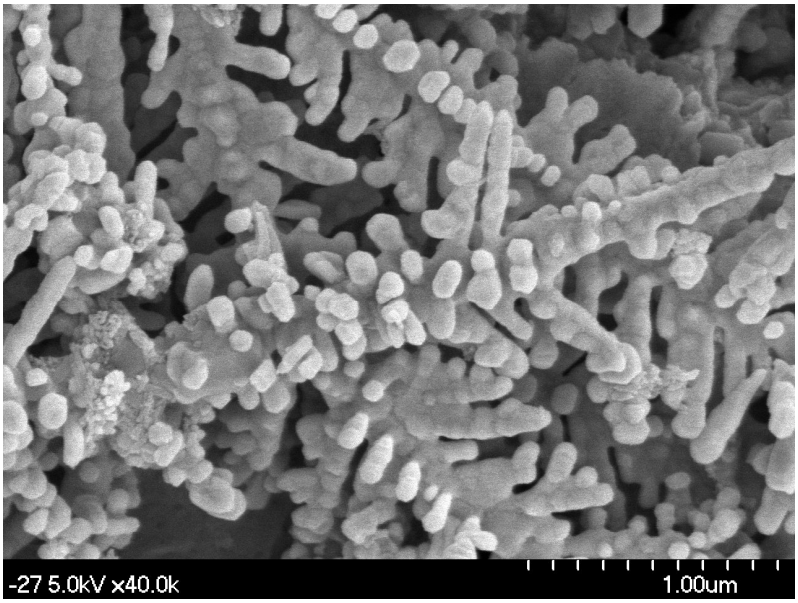

(b)

Fig. 2.

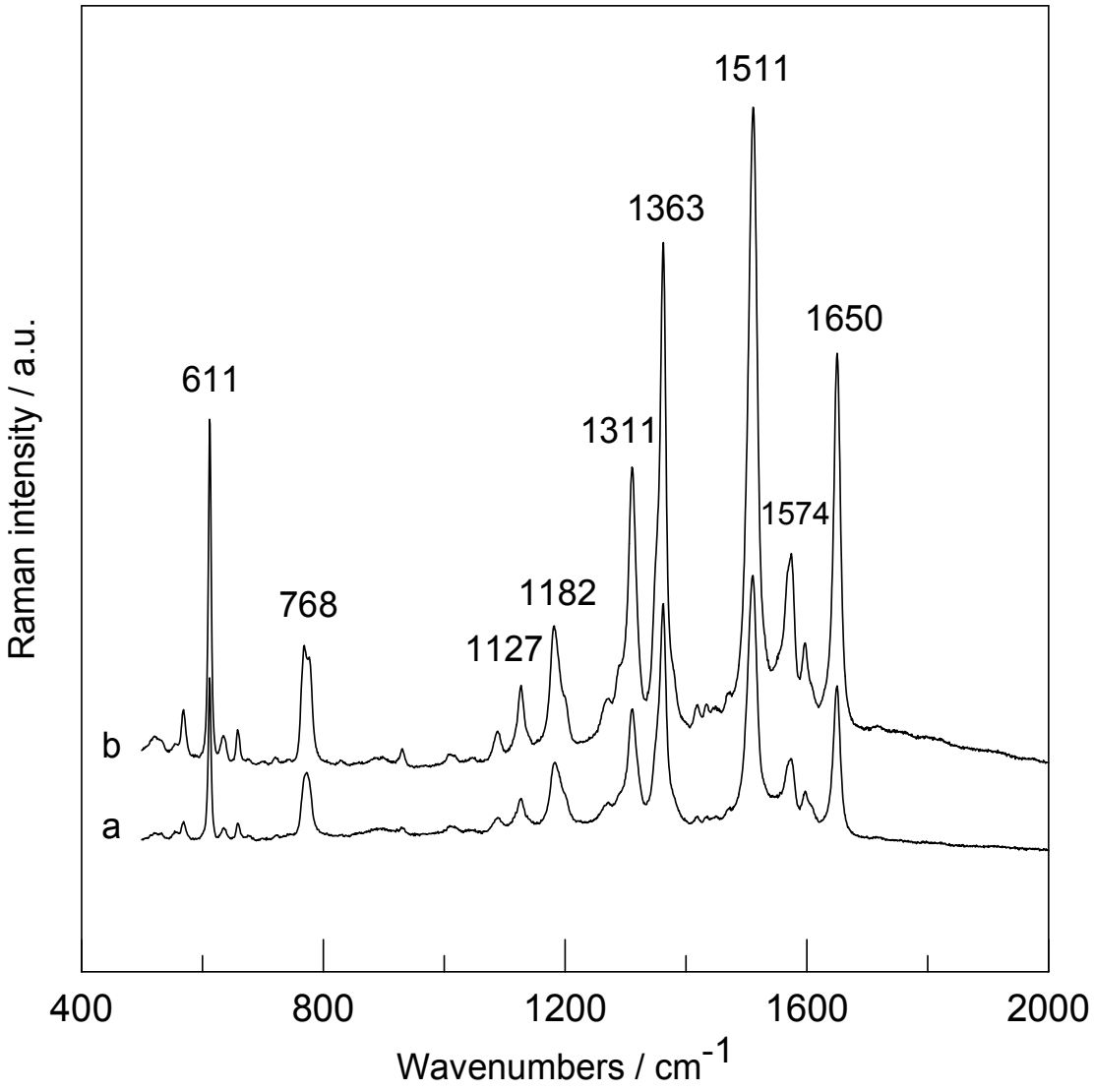

Fig. 3.

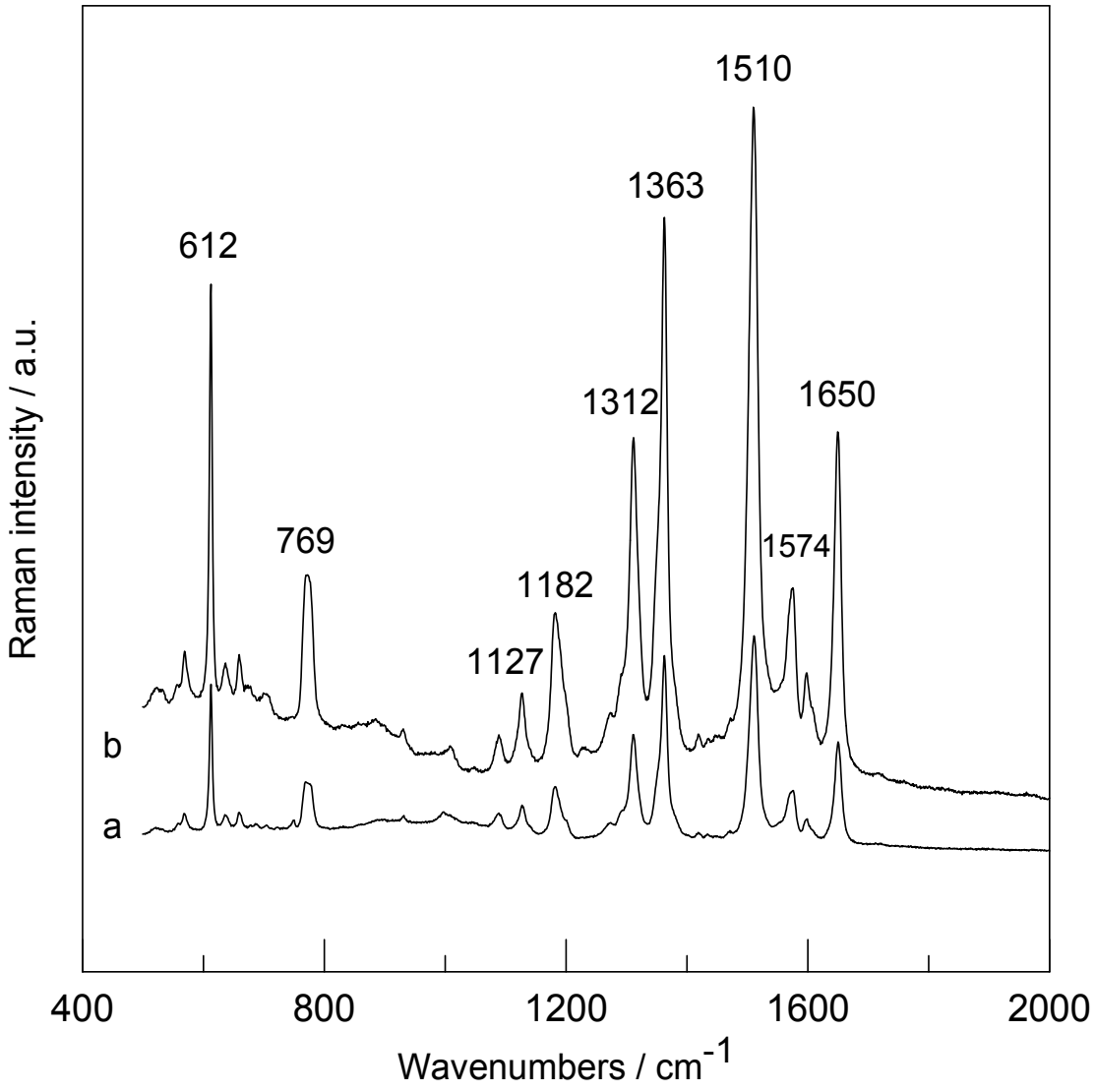

Fig. 4.

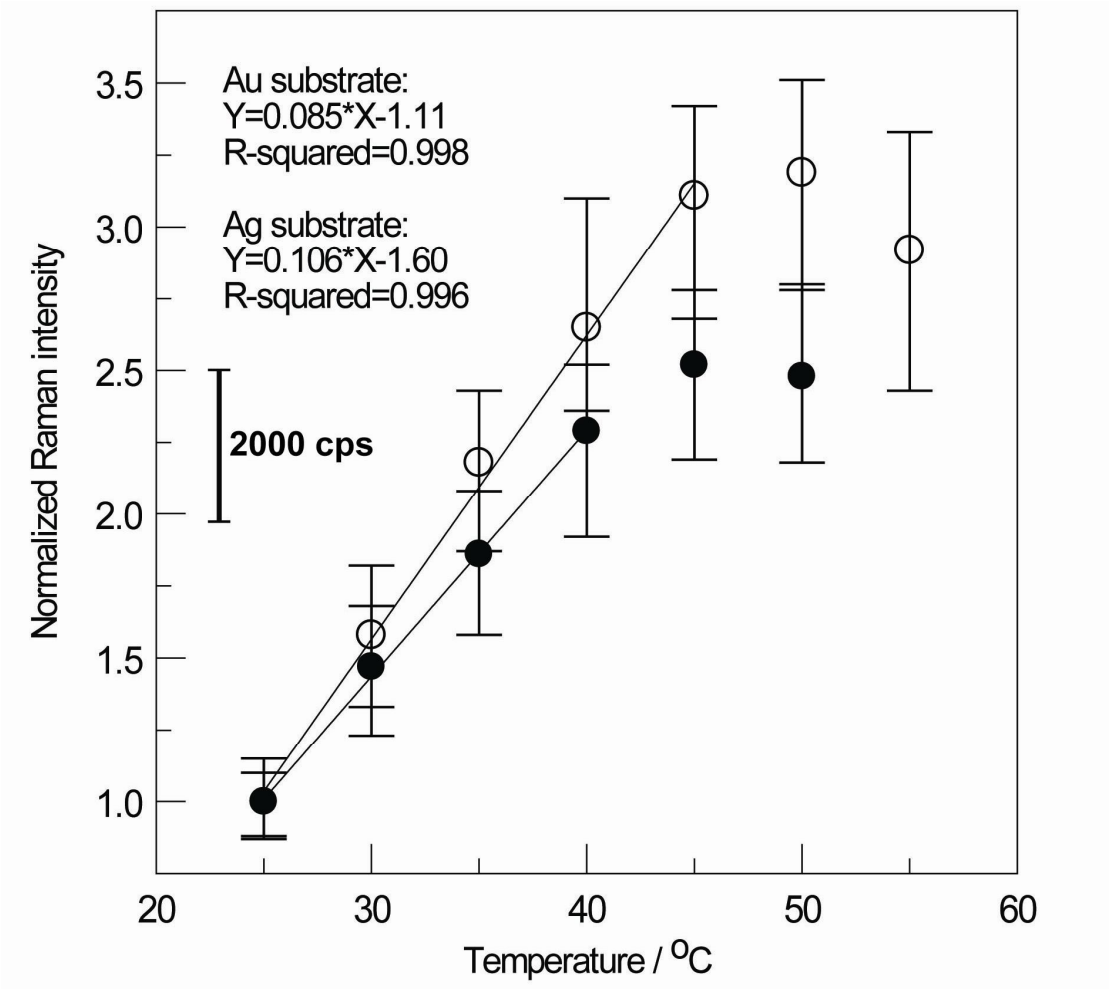

Fig. 5.

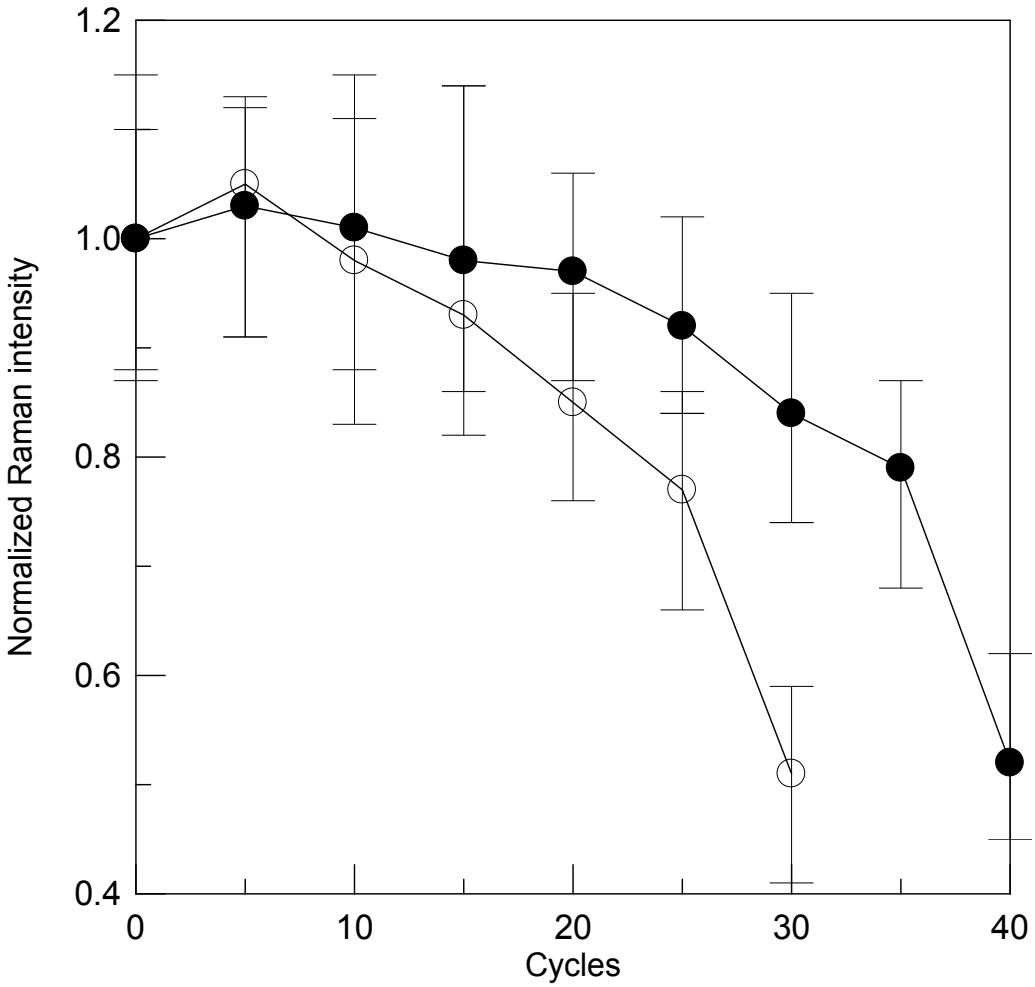

Fig. 6